Journal of Hydroscience and Hydraulic Engineering
Vol. 1, No. 2, November, 1983, pp.17-31.

EXPERIMENTAL ANALYSIS ON THE OPEN CHANNEL FLOW IN RECTANGULAR CONTINUOUS BENDS

By

Nobuyuki Tamai

Professor, Department of Civil Engineering
University of Tokyo, Bunkyo-ku, Tokyo, Japan

Kouji Ikeuchi

Engineer, Upper Arakawa River Office, Ministry of Construction, Kawagoe-shi, Saitama, Japan

Akira Yamazaki and Ali A. Mohamed

Graduate Students
University of Tokyo, Bunkyo-ku, Tokyo, Japan

SYNOPSIS

Experiments were performed in a flume which has a similar planimetric shape as rivers and ten consecutive bends. Flow conditions are selected to satisfy conditions that the water depth is much smaller than the radius of curvature of a bend and that the Reynolds number is fairly large.

Variations of the transeverse surface gradient and the primary and the secondary velocity fields along a bend are clarified and it is shown that there exists no fully developed zone in case of continuous bends. The effect of a residual secondary circulation of a preceding bend plays an important role in the flow pattern in vertical planes.

The relative magnitude of terms in the longitudinal and the transverse momentum equations is analyzed by numerical differentiation of measured velocity.

INTRODUCTION

A meandering channel is one of the typical features of rivers. Helical flow caused in a curved reach produces a deep scour hole and superelevation along the outer bank, which threatens the security of bank during floods. The three- dimensional flow structure in river bends, however, has not yet been completely clarified.

Both theoretical and experimental approaches in previous studies lay a stress mainly on fully developed zone of the secondary current and on a strongly curved single bend. It is not so easy to find out published data for a single bend which were obtained under the similar values encountered in actual rivers in terms of H_o/B_o and H_o/r_c, where H_o= the representative water depth; B_o= the width of the channel and r_c= the radius of the curvature along the centerline. In rivers these ratios are sufficiently small compared with unity. As far as the authors know, a comprehensive experimental data which satisfy the condition aforementioned cannot be found except in Rozovskii's book (9) in an accessible manner.

Furthermore, there are continuous bends in rivers. But only a few experiments were performed in continuous bends, e.g., by Yen (15), Hooke (2), and Kinoshita (5), satisfying the condition that H_o/r_c is sufficiently smaller than unity. In field observation (3 & 14) outlines of transitional flow structures from an upstream bend to a downstream bend are described.

The objective of this paper is to provide comprehensive quantitative data under the same conditions as those in rivers utilizing continuous bends. The experi-

ment is also performed to obtain better basic data which are able to be used for the sensitivity check among various theoretical approaches. In order to avoid the complexity raised by boundaries, a rectangular, fixed bed model is used in the experiment .

Major part of this paper has been originally published in the references (12 & 13).

EXPERIMENTAL APPARATUS AND PROCEDURE

Design of Test Flume

Hydraulic conditions of the experimental flume and experimental runs are determined referring to field observation. Leopold and Wolman (7) published the result of field measurements for wave length of the meander, λ , as follows:

$$\lambda = a\, B_o \qquad (1)$$

where the value of the coefficient a is in the range between 7 and 11.

Schumm (10) summarized the results for the width to depth ratio for more than 50 natural rivers. The result falls into two zones, that is,

$$\frac{B_o}{H_o} = 7 \text{ to } 10 \quad , \quad \text{and} \quad 20 \text{ to } 50 \qquad (2)$$

The ratio is greatly influenced by sediment type and it is reported that the width-depth ratio tends to show smaller values if silt-clay ratio in sediment is large.

The radius of the curvature of centerlines of streams is obtained in relation to the width (7).

$$\text{mean value of } \frac{r_c}{B_o} = 2.3 \qquad (3)$$

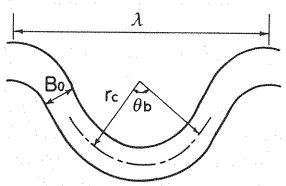

Fig. 1 A meandering reach and symbols

Yen (15) noted that the mean value of r_c/B_o falls in the range of 5 to 10. Yen obtained larger values than that in Eq. 3 because he payed attention to the trace of thalwegs in the Mississippi and the Misouri Rivers for average low-water conditions.

As for the central angle of bends, Θ_b , we can utilize Yen's (15) data. A cumulative frequency curve exceeds 50% at the value shown in Eq. 4.

$$(\Theta_b)_{50} = 80^o \text{ to } 100^o \qquad (4)$$

Although a sine generated curve has been frequently used in analytical studies to express the locus of the centerline of meandering streams, the experimental flume of this study is composed of a circular channel and a straight channel in unit bend considering the convenience and the preciseness of the model making. The planimetric geometry of the experimental flume was chosen as in table 1.

As for the length of the tangent reach Yen (15) gave a cummulative frequency curve which showed 50% for the following values.

$$(l/r_c)_{50} = 0 \text{ to } 0.9 \qquad (5)$$

The ratio adopted in this experiment falls also in this range, that is, $l/r_c = 0.5$.

Thus, the planimetric geometry of the flume utilized in this experiment well represents the shape of streams encountered in the field satisfying approximately the criteria stated in Eqs. 1 through 5.

The planimetric shape of the experimental flume is shown in Fig. 2. The comparison of the centerline with a sine generated curve in Fig. 2 shows that they agree cosiderably well with each other.

The longitudinal slope of the bed is chosen to give a moderate value of the Froude number. According to the report of Leopld and Maddock (6) the Froude number

Table 1 Dimensions of the experimental flume

radius of curvature of the centerline	r_c = 0.60 m
central angle of a bend	θ_b = 90°
length of the tangent reach between unit bend	ℓ = 0.30 m
width of the flume	B_o = 0.30 m
wave length of the meander	λ = 2.12 m
design representative flow depth	H_o = 0.03 m

in rivers is less than 0.5. The bed material of the flume is mortar and the Manning's roughness coefficient is estimated in the range of 0.012 to 0.014. Considering that the representative flow depth is 0.03 m, the bed slope is determined to be 1/1000 along the centerline of the flume. In lateral direction there is no inclination in the bed. Estimated value of the Froude number is 0.43 .

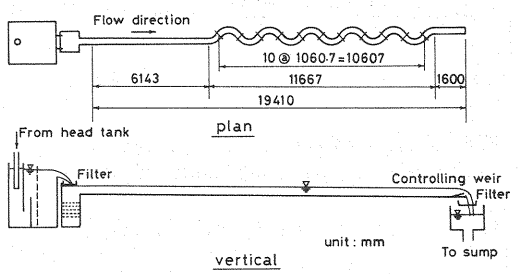

Fig. 2 The shape of a unit bend and the comparison with a sine-generated curve

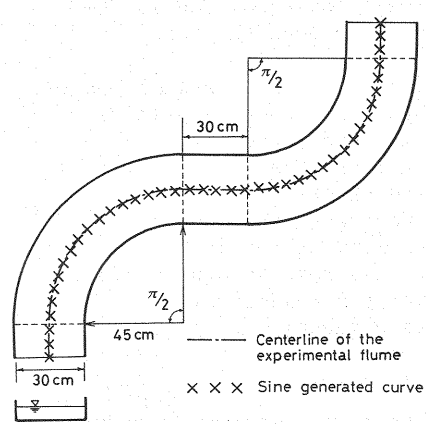

Fig. 3 The arrangement of the experimental flume

The arrangement of the experimental flume is shown in Fig. 3. We have ten consecutive bends and neighboring two bends are connected in anti-phase. The flume has two 45°-bends at the tail of these consecutive bends and also it has two straight reaches further to connect with head and tail tanks.

Experimental Procedure and Instrumentation

In this experiment the number of measuring points is very large (about four hundred points in one unit bend, that is, four thousand points in total ten bends). Since the measurement cannot be completed in a day, the same experimental condition should be repeatedly obtained. In order to insure the experimental condition, the following two steps were checked at the beginning of each run. First, static pressure at the mid-section of the tangent reach of neighboring bends was measured to make the water surface gradient coincide with the bed slope. Secondly, the water surface level of a tank at the head of this flume was measured by a point gage to get the same discharge throughout the series of experiments.

Transverse water surface profiles were measured by a static pressure probe composed of rake-shaped seven tubes. The outer diameter of each tube is 2 mm and the probe is considered to give negligible effect on the variation of the water surface. The direction of the flow at different points in the stream was measured

by a tuft method. When the fluctuation of a silk thread was intense, a longer averaging time was used. At points where the measured data deviated very largely from a smooth empirical curve, the measurement was performed again after the measurement in one section was completed.

A current meter of propeller-type was utilized for the velocity measurement. The diameter of the propeller is 3 mm. The rotating axis of the propeller was set in the direction of the flow measured by the tuft method. The longitudinal and the lateral components of flow are computed utilizing the flow direction at each point. The current meter was calibrated in a small towing tank. The electric output of the current meter was influenced by the depth of submergence of water. The calibration formula was derived from the measured values for some different depths of submergence up to the maximum depth encountered in the experiment.

Hydraulic Conditions

Quasi-normal flow condition was obtained for each run by the method mentioned in the preceeding section. Tested cases are listed in Table 2. Figure 4 shows that the average water depth through ten bends coincides with the bed slope and that quasi-normal flow condition is established throughout the bend region.

Flow features at the same phase in each bend are repeated precisely through ten bends except two 45°-bends located at the head and the tail of the channel. Therefore, the phase average was taken to increase the reliability of the data. In Case 1 measurements were perform for all the ten bends, while in Case 2 measurements were performed in the middle part of the flume, i.e., from the 4th bend to 7th bend from the upstream.

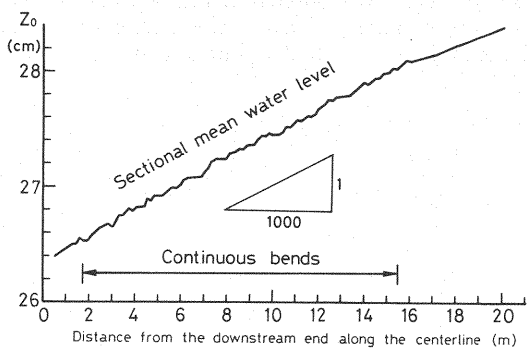

Fig. 4 Variation of the water surface level along the longitudinal direction

Table 2 Hydraulic Conditions

Case	mean water depth H_o in cm	width-depth ratio	mean velocity V in cm/s	Darcy-Weisbach friction factor f	F_r	R_e
1	2.93	10.0	22.3	0.0115	0.42	5500
2	5.01	6.0	32.8	0.00916	0.47	13500

TRANSVERSE PROFILE OF THE WATER SURFACE

In Fig. 5 the transverse profile of the surface for Case 1 is shown. The naming of sections is designated in Fig. 6. In Fig. 5 the abscissa represents the transverse coordinate, n , taken from the centerline of the flume toward the outer bank (left bank in Fig. 6). Let I_n denote the transverse gradient of water surface . Figure 5 (a) shows that the transverse surface gradient is almost zero and the sign is minus at the mid-section of a tangent reach between two neighboring bends. I_n increases as the flow goes downstream and reaches to its maximum at the section around $\pi/6$ keeping the same value up to the section $\pi/3$. Then, I_n decreases gradually toward the mid-section of a next tangent reach. At the section

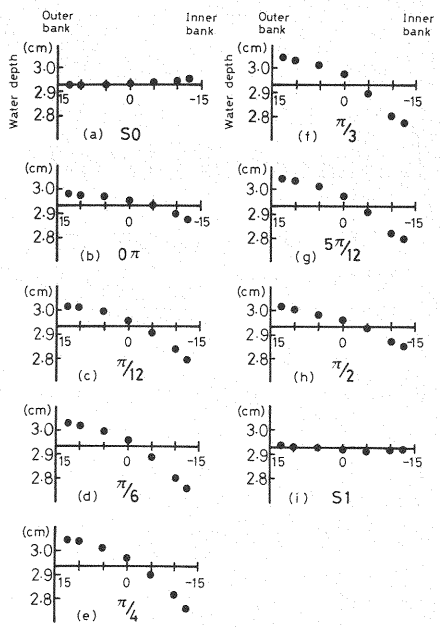

Fig. 5 The transverse water surface profile

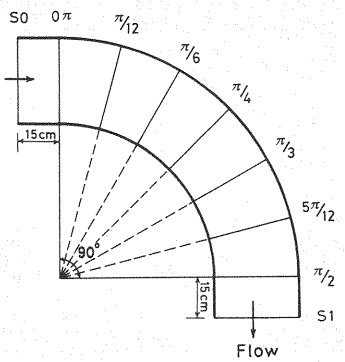

Fig. 6 Naming of measuring sections

S_1 (the exit of a unit bend), we have the opposite profile to that observed at the section S_o (the entrance of a unit bend).

It is seen that the variation of the transverse water surface shows no phase lag with the advancement of the flow along a bend. In Case 2 the similar features were observed. But the variation near the entrance and the exit regions were more intense than that observed in Case 1.

PRIMARY VELOCITY FIELD

Vertical Distribution of the Primary Flow

In the present study the velocity component parallal to the tangent of the centerline of the flume is termed the primary flow. In fig. 7 the phase averaged value of the primary component along the verticals is shown for Case 1. From Fig. 7 we can clearly see that there is a characteristic velocity distribution in which the maximum appears at the middle of the depth or near the bottom. This barrel-type velocity distribution seems to be a typical feature of the flow in a continuous bend with a flat bed, since the similar result was also observed in Case 2 and appeared in Yen's experiment (15).

The barrel-type profile is observed near the outer bank in the entrance region to the bend. As the flow advances to the middle section of the bend, this type of the profile is seen near the centerline of the section. As the flow proceeds further downstream, the barrel-type profile is seen near the inner bank in the exit region of the bend.

The transversely averaged value of the primary velocity at the same level shows the similar barrel-type profile. This is also reported by Siebert and Gotz (11) in their experimental flume of 3 consecutive bends with rectangular cross section.

Figure 7 is the result in Case 1 and the result in Case 2 reconfirms the conclusion mentioned above.

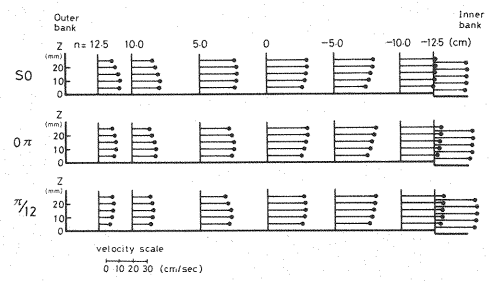

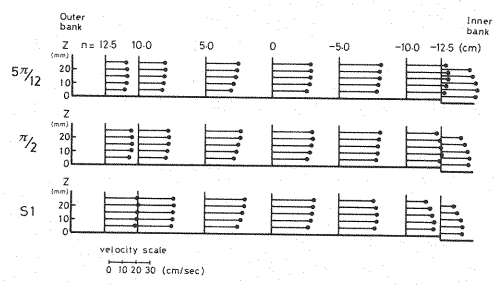

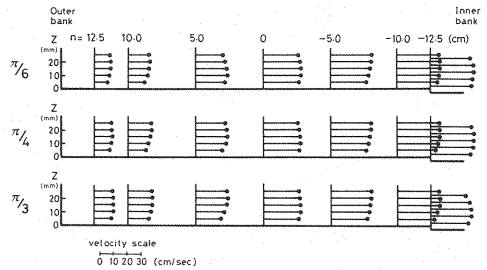

Fig. 7 Velocity distribution of the primary component

Transverse Distribution of the Depth-Averaged Primary Flow

Let $\bar{u}_s$ denote the depth-averaged primary velocity. Transverse distribution of $\bar{u}_s$ is assumed to follow Eq. 6.

$$\bar{u}_s = \alpha \left(\frac{r}{r_c} \right)^m \qquad (6)$$

where α and m = constants and r = local radius of curvature at observed point.

The variation of the value of m is given in Fig. 8. The exponent m was obtained at each section by least-square-method. In Fig. 8 the measured result by Rozovskii (9) and Yen (15) are depicted for comparison. The present result shows that m takes the minimum value where the bend angle reaches around $\Pi/3$. The general tendency of the present work is similar to that obtained by the rearrangement of Yen's data (15) which were measured in the second one of two consecutive bends.

On the other hand, Rozovskii's experiments were carried out in a single bend central angle of which was 180^o. In Rozovskii's work there is a zone where the exponent m remains constant. In the range of Θ between 40^o and 100^o, m is nearly equal to -0.8, which means a fully developed flow condition seems to be realized in this region. In his result the range where Θ exceeds 180^o means a straight reach connectd to the bend. In this straight reach m is kept to be a value larger than 0.5, which means the influence of bend remains effective to a considerablly lower reach in case of a single bend.

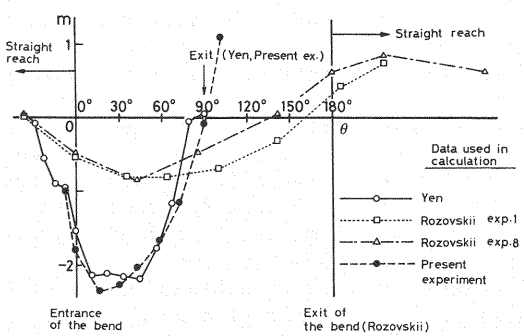

Fig. 8 The longitudinal variation of the exponent in Eq. 6

The observed results shown in Fig. 8 indicate that in continuous bends which are frequently encountered in rivers with the central angle of about 90^{o}, transverse distribution of the depth-averaged primary flow does not show a fixed functional form. It is also shown that the sign of the exponent m is minus in almost all the region throughout bends, which means that the primary velocity near the inner bank is larger than that near the outer bank. The same transverse profile is reported in the second bend of Mosonyi et al's (8) experiment. This seems to be a general aspect in the flow through a bend with fixed, flat bed.

SECONDARY VELOCITY FIELD

Vertical Distribution of Secondary Currents

In Fig. 9 phase-averaged value of the lateral velocity component is shown at each location. Since a propeller-type current meter was used, we could not measure the velocity at locations which are very close to the water surface and the bottom. Measurements of the direction of flow, however, can be done near the boundaries. Variation of the flow direction is similar to that reported by Yen (15). Hereafter, discussion is developed based on the measurement of both secondary currents and the flow direction.

It is clearly seen in Fig. 9 that the lateral velocity is negative(towards the inner bank) near the water surface and is positive (towards the outer bank) near the bottom at the entrance region of the bend. This is a completely opposite flow pattern reported for the fully developed zone. This is the direct consequence of a remaining secondary current generated in the preceding bend. Between the sections $\Pi/12$ and $\Pi/4$ the direction of the secondary current near the bottom changes towards the inner bank, while the water particle near the water surface is kept unchanged to travel towards the inner bank. Therefore, vertical profile of the secondary currents crosses zero twice in the water depth. Between the sections $\Pi/6$ and $\Pi/3$ the intensity of the negative component (to the inner bank) of lateral

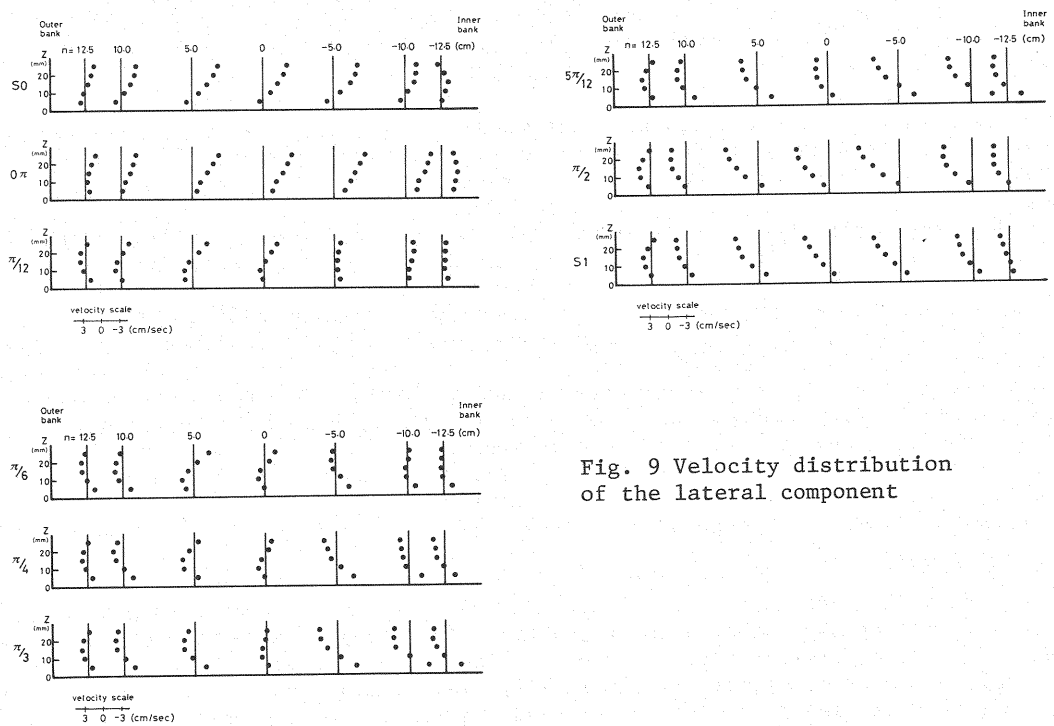

Fig. 9 Velocity distribution of the lateral component

velocity begins to decrease. As the flow proceeds to the section between $5\Pi/12$ and S_1, the secondary flow reaches to a new stage. In this exit region we can observe the outward lateral flow near the surface and the inward flow near the bottom.

Figure 9 was derived from the measurement in Case 1, and Case 2 provided the similar result.

Secondary Circulation Along the Bend

Based on the result shown in Fig. 9, we depicted Fig. 10 which schematically shows the variation of secondary flow pattern along the continuous bend. At the section S_o the secondary currents developed in a preceding bend occupies the whole section. The secondary currents produced in a present bend begins to develop at the section $\Pi/12$ (about one sixth of the total length of a bend) near the bottom. In the midsection of a bend two oppositely circulating secondary currents coexist sharing a comparable area in the section. Then, in the exit region a new secondary current finally occupies the whole section.

It is seen that the growth of the spiral flow in a continuous bend is strongly affected by the residual spiral from the preceding bend, while the decay of the spiral flow from the preceding bend is accelerated by the growth of a new spiral. It is also shown that there is no fully developed zone for secondary currents in continuous bends, that is, the flow pattern varies repeatedly in the longitudinal direction and does not remain unchanged along the bend.

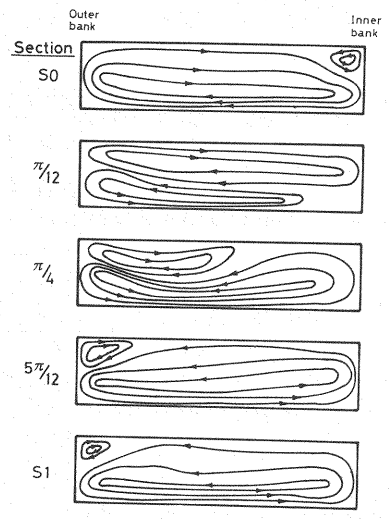

Fig. 10 Schematic representation of the change of the secondary circulation

ORDER ESTIMATION OF THE TERMS IN MOMENTUM EQUATIONS

The longitudinal variation and the relative magnitude of each term in momentum equations are considered on the basis of order estimation computed from measured data. A general orthogonal curvilinear coordinate system is utilized to describe momentum equations. s-axis is taken along the centerline of the flume and n-axis is taken perpendicular to s-direction. Velocity components in s and n directions are denoted by u_s and u_n, respectively. In case of a cylindrical coordinate, $ds = r\,d\Theta$ and r = constant are applied where r is a local radius of curvature. If it is assumed that the radius of the curvature of the centerline of a flume varies as $1/r = (1/R)\cos \omega s$, the sine-generated curve well reproduces the locus of actual meandering channels.

Since the unit of the experimental flume consists of a circular reach and a straight reach, a cylindrical coordinate is best to express the fixed boundary. But the radius of curvature at the connection between a circle and a straight line varies discontinuously and a pathline of a fluid particle cannot follow this sudden change. Therefore, the analysis which follows a streamline of the flow is also performed utilizing a sine-generated curve.

Momentum Equations

If flow in a bend satisfies the condition $H_o/r_c \ll 1$, the pressure distribution is well approximated to be hydro-static (9). Paying attention to the condition $H_o/r_c \ll 1$, smaller terms in the Reynolds stress tensor are neglected. Since vertical component of velocity is negligibly small except the wall region (9), the vertical velocity is assumed to be zero and the central part of a section is considered. Under these assumptions, momentum equations in s and n directions are given in the following form (4) (as for symbols see Appendix-Notation):

$$u_s \frac{\partial u_s}{\partial s} + u_n \frac{\partial u_s}{\partial n} + \frac{u_s u_n}{r} + \frac{1}{\rho}\frac{\partial p}{\partial s} = \frac{\partial}{\partial z}\left(\varepsilon \frac{\partial u_s}{\partial z}\right) \quad (7)$$

$$u_s \frac{\partial u_n}{\partial n} + u_n \frac{\partial u_n}{\partial n} - \frac{u_s^2}{r} + \frac{1}{\rho}\frac{\partial p}{\partial n} = \frac{\partial}{\partial z}\left(\varepsilon \frac{\partial u_n}{\partial z}\right) \quad (8)$$

Finite Difference Scheme for Momentum Equations

In Case 1 velocity measurements were performed at 30 points in a section and 9 sections along a bend. Observation points are shown in Fig. 11. Magnitude of each term in Eqs. 7 and 8 at the center of a rectangle are computed from the measured values at four vertices of a rectangle by a finite difference scheme. The right hand sides of Eqs. 7 and 8 consist of second derivative. Therefore, it is supposed that the numerical derivative produces large error. To evaluate the right hand side, the vertical velocity distribution and the eddy viscosity are approximated by continuous functions. $u_s(z)$ is expressed by a cubic equation and the equation $\varepsilon = (1/13)\, u_* H_o$ is utilized (see Engelund (1)). u_n is given by $u_n = \delta u_s$ were δ is the angle between a velocity vector and s-axis and tan δ is approximated by δ . A cubic function to describe the measured distribution of $u_s(z)$ was derived by a regression analysis.

Longitudinal Momentum Equation

The magnitude of each term of Eq. 7 is calculated at 30 mesh-points shown in Fig. 11 at the mid- section between 9 measuring sections shown in Fig. 6. Along a vertical line the measuring points are set at an interval of 0.5 cm from the bottom toward the water surface. In the range of the present experiment, longitudinal variation appears to be independent of the vertical level. The observed result at three points (1-3), (3-3), and (6-3) (see Fig. 11) is shown in Fig. 12. In the present study the behavior of flow very close to the bottom is out of scope because the data in this zone could not be obtained due to the restriction of the current meter.

In Fig. 12 the abscissa explains the central angle of rotation along a bend. The regions less than zero degree and larger than 90 degrees correspond to straight reaches between the neighboring circular reach. It is seen that interia terms ($u_s \cdot \partial u_s/\partial s$ and $u_n \cdot \partial u_s/\partial n$) and the

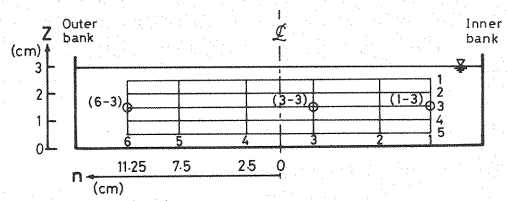

Fig. 11 Measuring of velocity in a section

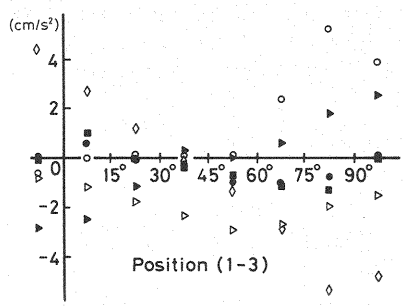

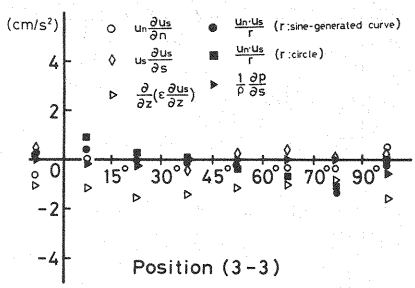

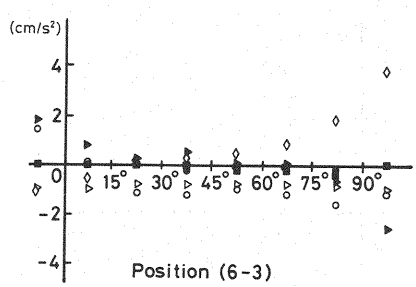

Fig. 12 Relative magnitude of the terms in the longitudinal momentum equation

longitudinal component of the centripetal force ($u_s u_n/r$) are not always small in magnitude. These nonlinear terms are prevailing at the exit region of a bend. There is no significant difference between two results of the evaluation of the term $u_s u_n/r$ where the centerline of the flume is taken as a circle in one case and as a sine-generated curve in another case. If the velocity measurement and the numerical differentiation are sufficiently precise, the sum of four terms in the left hand side coincides rigorously with the right hand side in Fig. 7.

It is described in Fig. 12 that this balance is approximately statisfied. The residual seems in the order of unit scale in ordinate. The error is caused in the process of numerical differentiation from the measured data. Although it should be admitted that certain amount of error is involved in the representation of Fig. 12, general trend and relative magnitude among the terms in the momentum equation are considered to be explained in the present study.

Transverse Momentum Equation

The variation of each term of Eq. 8 is shown in Fig. 13. The described results were obtained at the same measuring points at the mid-depth as in the case of Fig. 12. The depthwise variations of the magnitude of the pressure and the centripetal terms are considered to be small except the wall region close to the bottom. If the hydrostatic pressure field prevails, there is no depthwise variation the transverse pressure gradient. In turbulent flows the velocity distribution is fairly uniform in the fully developed zone. This means that the vertical distribution of the centripetal force is also fairly uniform.

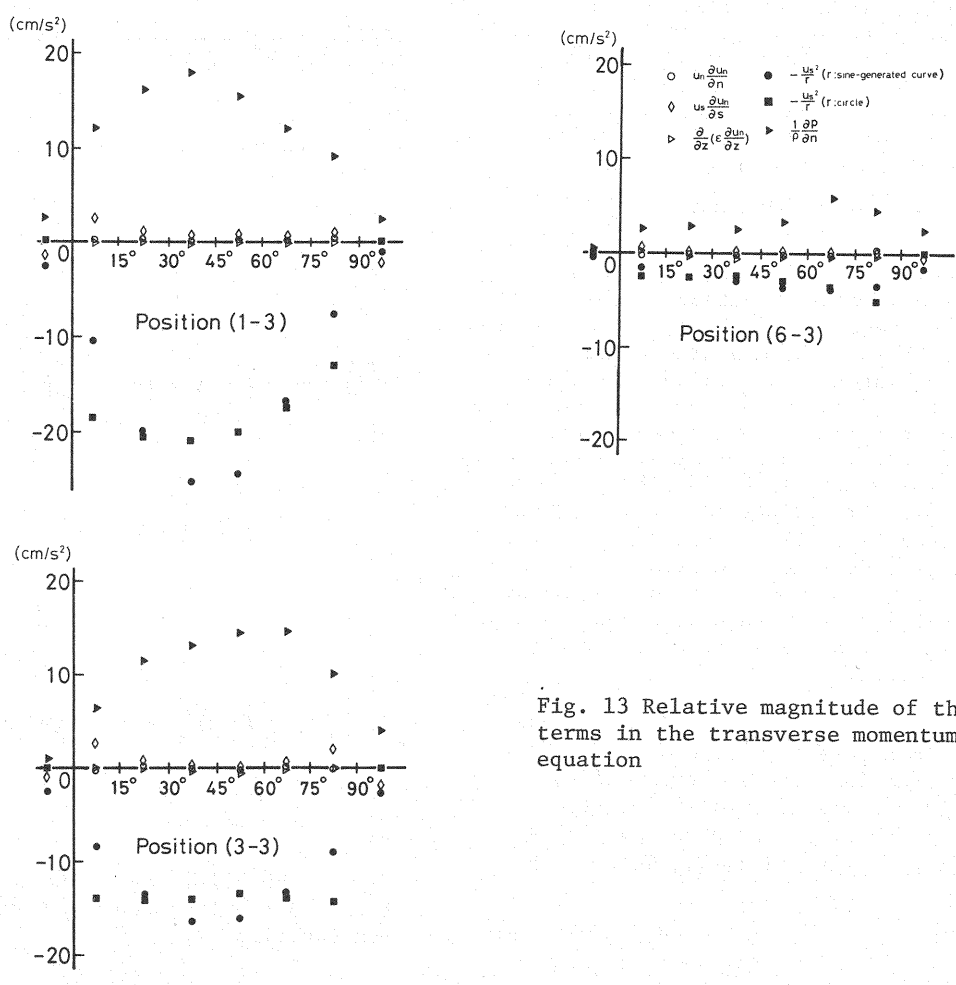

Fig. 13 Relative magnitude of the terms in the transverse momentum equation

Figure 13 shows that the pressure term and the centripetal term are the two major components in the momentum balance in the transverse direction. Around the apex of a bend the magnitude of these two terms reaches its maximum. $u_s \cdot \partial u_n / \partial s$, one of the inertia terms, becomes relatively large at the entrance and the exit regions. This term may be important to account for the evolution and the decay of secondary flows.

The transeverse shear term is negligible throughout a bend. Consequently, the shear term is negligible at all sections in the transverse momentum equation. The present experiment was performed in a hydraulically smooth flume with mortar bed. A separate measurement should be made to discuss the details of the shear near the rough wall.

As for the radius of curvature, it is concluded that near the entrance and the exit the estimation based on a sine-generated curve gives better results in counting the balance of the sum of all terms in Eq. 8. On the other hand, the estimation based on a circle which follows an actual shape of the side boundary gives better results in the balance in the central part of a bend. According to these results the shape of the streamlines is considered as follows: First, at the junction between a straight reach and a circular reach water particle cannot follow the discontinuous change in the radius of curvature, and graually changes its course. Secondly, in the central part of a bend the shape of streamlines looks like a circle. In general, convergency of streamlines toward the outer bank in the upper half reach of a bend and toward the inner bank in the lower half reach are seen.

CONCLUDING REMARKS

Present experiments are performed in the flume which has a similar planimetric shape as rivers and satisfies the condition that the water depth is much smaller than the radius of curvature of its bend. It is confirmed that equilibrium condtion was realized repeatedly in ten consecutive bends. The data presented herein are obtained through the average of ten data which were measured at the same locations from phasic point of view in bends. This phase averaging increases the preciseness of data. Conclusions derived from the present analysis are as follows:

1) The transverse water surface profile becomes nearly horizontal at the entrance and exit of a bend. Variation of the transverse surface gradient begins and ends up with no phase lag as the flow enters into and passes away from a bend.
2) The maximum primary velocity appears at certain distance below the water surface. This barrel-type velocity distribution appears near the outer bank in the entrance region of a bend and then the location of the appearance gradually moves toward the inner bank as the flow proceeds downstream to the exit region.
3) In a flow through continuous bends both primary and secondary flow fields continuously vary along a bend. There exists no fully developed zone in the present study.
4) In case of continuous bends, a residual secondary circulation of a preceding bend prevails in wide range of a next bend. A new secondary circulation is initially generated near the bottom and gradually grows overcoming a previously existing one. After flow goes through about two thirds of the bend, a new secondary flow developed in the bend occupies the whole section.
5) In the longitudinal momentum equation inertia terms and the longitudinal component of the centripetal force are comparably large. The magnitude of these terms varies along a bend, which is supposed to create the variation of the primary and the secondary velocity fields mentioned in previous items.
6) In the transverse momentum equation, transverse pressure gradient and the centripetal force are influential. At the entrance and the exit regions an inertia term concerned with the longitudinal variation of the lateral velocity becomes relatively large. The shear term is negligibly small in this direction in the whole region of a bend.

ACKNOWLEDGMENTS

The authors wish to express their sincere gratitude to Dr. Ryosaku Kinoshita for his instructive discussion on the field observations he performed. The first auther wishes to thank Prof. Kazuo Ashida at Kyoto Univ. and Prof. Nobuo Shuto at Tohoku Univ. for their assistance given through Task Committee on ' Three-dimensional nature of flood flows and bar formation' organized by Committee on Hydraulics of JSCE. The authors are also indebted to Assoc. Prof. Syunsuke Ikeda at Saitama Univ. for introducing Hooke's paper and to Mr. Yusuke Hirosawa for the assistance given in the preparation of experiments and drawings.

REFERENCES

1. Engleund, F. : Flow and bed topography in channel bends, Proc. ASCE, Vol. 100, HY11, pp. 1631-1647, 1974.
2. Hooke, R.L. : Shear-stress and sediment distribution in a meander bend, UNGI-report 30, Univ. of Uppsala, 58p., 1974.
3. Jackson, R. G., II. : Velocity-bed-form-texture patterns of meander bends in the lower Wabash River of Illinois and Indiana, Geol. Soc. Amer., Bulletin, Vol. 86, pp. 1511-1522, 1975.
4. Kalkwijk, J. P. Th. and H. J. de Vriend: Computations of the flow in shallow river bends, J. Hyd. Research, IAHR, Vol. 18, No. 4, pp. 327-342, 1980.
5. Kinoshita, R. : Similarity law on a meandering channel of a mild slope three-dimensional experiment, The Ishikari River Construction Bureau, 164 p., 1974 (in Japanese).
6. Leopold, L. B. and T. Maddock : The hydraulic geometry of stream channels and some physiographic implications, U.S.G.S. Prof. Paper 252, 57 p., 1953.
7. Leopold, L. B. and M. G. Wolman: River meanders, Geol. Soc. Amer., Bulletin, Vol. 71, pp. 769-793, 1960.
8. Mosonyi, E., H. Meckel and G. Meder: Etude de developpement du courant spiral dans des courbes consecutives d'un canal, Proc. 16th Congress, IAHR, Vol. 2, pp. 347-355, 1975.
9. Rozovskii, J. L.: Flow of Water in Bends of Open Channels, Israel Program for Scientific Translations, 233 p., 1961.
10. Schumm, S. S.: The shape of alluvial channel in relation to sediment type, U.S. G.S. Prof. Paper 352-B, 30 p. 1960.
11. Siebert, W. and W. Gotz: A study on the deformation of secondary flow in models of rectangular meandering channels, Proc. 16th Congress, IAHR, Vol. 2, pp. 141-149, 1975.
12. Tamai, N., K. Ikeuchi and A. Yamazaki: Experimental analysis of the open channel flow in continuous bends, Proc. Japan Soc. Civil Eng., No. 331, pp. 83-94, 1983 (in Japanese).
13. Tamai, N., A. A. Mohamed: Experimental study on the development of depth-averaged flow in rectangular continuous bends, Proc. 27th Jap. Conf. on Hydraulics, JSCE, pp. 85-90, 1983.
14. Thorne, C. R. and R. D. Hey: Direct measurements of secondary currents at a river inflexion point, Nature, Vol. 280, pp. 226-228, 1979.
15. Yen, B. C.: Characteristics of subcritical flow in a meandering channel, Inst. of Hyd. Research, The Univ. of Iowa, 77 p., 1965.

APPENDIX 1 - PHASE AVERAGED WATER DEPTH (unit: cm)

Symbol	n(cm) / Section	1	2	3	4	5	6	7
		12.5	10.0	5.0	0.0	-5.0	-10.0	-12.5
A	SO	2.96	2.95	2.94	2.94	2.93	2.93	2.93
B	OΠ	2.88	2.90	2.94	2.95	2.97	2.98	2.98
C	Π/12	2.80	2.84	2.91	2.96	3.00	3.01	3.02
D	Π/6	2.76	2.80	2.89	2.96	3.00	3.02	3.03
E	Π/4	2.77	2.81	2.90	2.97	3.02	3.04	3.05
F	Π/3	2.78	2.81	2.89	2.98	3.02	3.04	3.05
G	5Π/12	2.80	2.83	2.91	2.97	3.01	3.04	3.05
H	Π/2	2.86	2.87	2.93	2.96	2.99	3.01	3.02
I	S1	2.92	2.92	2.92	2.93	2.93	2.94	2.94

n: Distance from the centerline to the outer bank.

APPENDIX 2 - PHASE AVERAGED PRIMARY VELOCITY u_s (unit: cm/s)

Position	Distance from the bottom (cm) 2.50	2.00	1.50	1.00	0.50
A-1	24.55	25.03	24.55	24.25	23.27
A-2	26.62	26.85	26.10	25.64	24.89
A-3	29.68	29.00	27.37	26.18	23.99
A-4	29.85	29.80	29.29	28.32	26.31
A-5	25.79	27.41	27.71	27.40	26.12
A-6	15.08	17.71	19.37	20.76	20.13
A-7	10.14	12.77	15.39	16.70	16.40
B-1	28.66	28.94	28.78	28.34	26.94
B-2	30.28	29.89	28.95	28.70	27.29
B-3	31.37	29.73	28.36	27.04	24.82
B-4	29.81	29.98	28.81	27.71	25.55
B-5	21.57	23.56	25.31	25.26	23.28
B-6	12.81	14.50	16.47	17.68	17.00
B-7	10.58	12.38	13.24	13.24	11.79
C-1	30.27	31.49	31.52	31.04	29.73
C-2	31.18	31.65	31.01	30.72	29.46
C-3	30.89	30.36	29.02	27.95	26.16
C-4	27.38	28.15	28.42	27.73	26.07
C-5	18.74	20.54	22.77	23.09	21.56
C-6	13.33	14.62	15.29	14.91	13.44
C-7	10.35	11.53	11.05	9.98	8.36
D-1	29.99	32.33	32.39	31.73	30.67
D-2	31.60	32.16	32.18	31.41	30.05
D-3	30.95	30.48	29.60	28.28	26.70
D-4	25.55	27.01	27.94	27.94	26.24
D-5	19.60	21.62	22.86	23.19	21.25
D-6	15.24	16.02	15.53	14.49	12.49
D-7	11.40	12.14	12.02	11.10	9.80
E-1	30.40	32.44	32.36	31.65	29.74
E-2	31.14	31.89	31.77	30.43	28.37
E-3	30.29	30.11	29.18	28.03	26.47
E-4	25.39	26.38	27.12	27.57	26.27
E-5	21.74	22.62	22.96	21.90	19.12
E-6	16.72	17.16	16.22	14.80	13.07
E-7	12.40	12.87	13.19	12.92	11.45
F-1	25.85	28.91	30.28	30.24	27.95
F-2	31.15	31.94	31.55	29.97	27.60
F-3	30.28	30.24	29.60	28.67	27.34
F-4	26.31	26.85	27.31	27.48	26.19
F-5	22.83	23.45	22.77	20.84	18.35
F-6	17.65	17.87	17.51	16.72	15.02
F-7	13.35	14.15	14.30	14.23	12.96
G-1	21.43	23.41	25.90	26.88	25.30
G-2	28.79	30.77	30.53	28.97	27.58
G-3	31.15	30.19	29.68	29.06	27.92
G-4	28.35	28.61	28.23	27.52	25.48
G-5	24.53	23.67	22.51	20.99	18.85
G-6	19.49	19.55	19.20	18.45	17.29
G-7	15.32	16.14	16.30	15.97	14.84
H-1	14.85	17.49	19.93	21.46	20.89
H-2	21.80	23.96	25.17	25.77	24.03
H-3	30.30	29.55	28.90	28.54	27.52
H-4	29.47	30.13	28.97	27.91	25.98
H-5	26.67	26.12	24.38	23.12	21.41
H-6	22.54	22.76	22.30	21.86	20.47
H-7	19.61	20.28	20.26	19.86	18.57
I-1	10.17	12.90	15.44	16.79	16.40
I-2	14.68	17.42	19.27	20.88	20.26
I-3	25.66	27.71	28.29	28.12	26.89
I-4	30.16	30.42	20.97	29.07	27.04
I-5	29.80	29.45	27.80	26.58	24.46
I-6	26.53	27.01	26.32	25.82	25.13
I-7	24.33	25.19	24.74	24.32	23.37

APPENDIX 3 - PHASE AVERAGED SECONDARY VELOCITY u_n (unit: cm/s)

Position	Distance from the bottom (cm) 2.50	2.00	1.50	1.00	0.50
A-1	0.39	-0.52	-1.25	-0.73	0.09
A-2	-1.84	-1.68	-1.43	-0.36	0.77
A-3	-4.06	-3.63	-2.73	-1.16	1.10
A-4	-4.11	-3.46	-2.45	-1.24	0.58
A-5	-4.40	-3.65	-2.48	-1.10	1.04
A-6	-2.60	-2.23	-1.66	-0.48	0.91
A-7	-1.59	-0.99	-0.54	0.22	0.64
B-1	-1.85	-2.31	-2.45	-2.26	-1.88
B-2	-4.09	-3.56	-3.14	-2.04	-1.78
B-3	-5.07	-4.25	-3.49	-2.78	-1.81
B-4	-4.83	-4.18	-3.30	-2.19	-1.48
B-5	-4.48	-3.46	-2.51	-1.40	-0.79
B-6	-2.51	-2.04	-1.49	-0.69	-0.24
B-7	-1.63	-1.09	-0.50	-0.31	-0.64
C-1	-0.60	-0.54	-0.47	-0.33	-0.99
C-2	-1.14	-1.20	-0.85	-0.38	-0.46
C-3	-1.02	-0.60	-0.54	-0.46	-0.96
C-4	-2.31	-1.24	-0.27	0.46	0.14
C-5	-2.58	-1.15	0.60	1.43	1.23
C-6	-1.33	-0.27	0.63	0.82	-0.05
C-7	-0.10	0.86	0.87	0.32	-0.82
D-1	0.31	0.26	0.34	0.03	-1.40
D-2	-0.30	-0.18	0.37	0.10	-1.32
D-3	0.39	0.62	0.28	-0.79	-2.13
D-4	-1.81	-0.94	0.68	1.03	-0.01

Position	Distance from the bottom (cm)				
	2.50	2.00	1.50	1.00	0.50
D-5	-2.58	-0.67	1.03	1.92	1.33
D-6	0.18	1.08	1.18	0.46	-1.37
D-7	0.20	0.73	0.73	-0.05	-1.39
E-1	1.80	1.54	1.18	0.13	-1.70
E-2	1.36	1.15	0.95	0.46	-2.11
E-3	2.01	1.55	0.79	-0.74	-2.80
E-4	-1.09	-0.54	0.62	1.14	0.14
E-5	-0.60	0.79	1.90	1.59	-0.61
E-6	0.94	1.58	1.03	-0.20	-1.68
E-7	-0.05	0.64	0.79	0.17	-0.92
F-1	1.91	2.12	1.49	0.17	-2.53
F-2	2.54	2.74	2.16	-0.02	-3.15
F-3	2.96	2.67	1.69	-0.46	-3.09
F-4	-0.03	0.07	0.71	0.77	-0.23
F-5	1.06	1.75	1.79	0.54	-1.96
F-6	0.91	1.34	1.08	-0.33	-1.81
F-7	-0.29	0.62	0.89	0.46	-0.79
G-1	2.09	2.24	1.96	0.55	-2.32
G-2	3.79	3.60	2.56	0,35	-3.37
G-3	4.14	3.34	2.04	-0.14	-2.61
G-4	1.99	2.05	1.85	1.16	-0.76
G-5	2.66	2.55	1.82	0.22	-2.31
G-6	0.60	1.27	1.29	0.28	-1.47
G-7	-0.61	0.43	1.11	0.74	-0.54
H-1	2.57	2.45	2.40	1.75	0.01
H-2	4.66	4.80	4.26	2.90	0.56
H-3	6.84	6.15	4.51	2.75	0.17
H-4	5.50	5.16	4.20	2.96	1.00
H-5	5.50	4.97	3.67	2.34	-0.48
H-6	2.40	2.59	2.27	1.34	0.11
H-7	0.14	1.27	1.88	1.58	0.23
I-1	1.64	1.08	0.64	-0.12	-0.56
I-2	2.56	2.22	1.72	0.46	-0.91
I-3	4.36	3.64	2.43	0.99	-1.09
I-4	4.18	3.54	2.56	1.20	-0.61
I-5	3.99	3.53	2.84	1.17	-1.13
I-6	1.73	1.60	1.30	0.39	-0.77
I-7	-0.48	0.48	1.24	0.90	0.06

APPENDIX 4 - PHASE AVERAGED ANGLE BETWEEN VELOCITY VECTOR AND S- AXIS (unit: degree, A positive value means the flow toward the outer bank.)

Position	Distance from the bottom (cm)						
	surface	2.50	2.00	1.50	1.00	0.50	0.00
A-1	2.1	0.9	-1.2	-2.9	-1.7	0.2	2.9
A-2	-4.7	-4.0	-3.6	-3.1	-0.8	1.8	5.3
A-3	-9.6	-8.0	-7.2	-5.7	-2.5	2.7	5.9
A-4	-8.8	-7.9	-6.7	-4.8	-2.5	1.4	5.1
A-5	-10.8	-9.9	-7.6	-5.1	-2.3	2.3	5.4
A-6	-11.1	-10.0	-7.3	-5.0	-1.3	2.6	4.7
A-7	-12.5	-9.0	-4.4	-2.0	0.8	2.2	2.3
B-1	-3.1	-3.7	-4.6	-4.9	-4.6	-4.0	-5.3
B-2	-8.4	-7.8	-6.9	-6.2	-4.1	-3.7	-5.1
B-3	-10.0	-9.4	-8.3	-7.1	-5.9	-4.1	-5.6
B-4	-11.0	-9.4	-8.0	-6.6	-4.5	-3.3	-3.5
B-5	-14.8	-12.1	-8.4	-5.7	-3.2	-2.0	-1.6
B-6	-15.1	-11.4	-8.1	-5.1	-2.2	-0.8	-1.8
B-7	-13.8	-8.8	-5.0	-2.2	-1.4	-3.3	-6.0
C-1	-0.6	-1.1	-1.0	-0.8	-0.6	-1.9	-10.7
C-2	-2.4	-2.1	-2.2	-1.6	-0.7	-0.8	-10.0
C-3	-2.2	-1.9	-1.1	-1.0	-0.9	-2.1	-8.7
C-4	-5.9	-4.8	-2.5	-0.5	0.9	0.3	-4.4
C-5	-13.3	-8.0	-3.3	1.5	3.5	3.2	-2.0
C-6	-10.4	-5.7	-1.1	2.4	3.2	-0.2	-6.4
C-7	-5.7	-0.5	4.3	4.5	1.8	-5.8	-13.3
D-1	0.5	0.6	0.5	0.6	0.1	-2.6	-14.7
D-2	-1.1	-0.6	-0.3	0.7	0.2	-2.4	-14.5
D-3	0.8	0.7	1.2	0.6	-1.5	-4.5	-13.6
D-4	-4.9	-4.0	-2.0	1.4	2.1	-0.1	-6.6
D-5	-11.8	-7.5	-1.7	2.6	4.8	3.6	-6.2
D-6	-4.3	0.7	3.9	4.4	1.8	-6.3	-13.6
D-7	-3.8	1.0	3.5	3.5	-0.1	-8.1	-16.9
E-1	3.1	3.4	2.7	2.1	0.3	-3.3	-15.2
E-2	2.3	2.7	2.1	1.7	0.9	-4.2	-17.4
E-3	4.3	3.8	3.0	1.6	-1.4	-6.0	-17.1
E-4	-2.9	-2.4	-1.1	1.4	2.4	0.2	-7.4
E-5	-5.6	-1.5	2.0	4.7	4.2	-1.9	-10.2
E-6	-0.3	3.3	5.3	3.7	-0.8	-7.4	-16.4
E-7	-4.9	-0.2	2.9	3.4	0.8	-4.6	-14.9
F-1	3.5	4.2	4.2	2.8	0.3	-5.2	-14.9
F-2	4.6	4.7	4.9	3.9	0.0	-6.5	-18.3
F-3	6.2	5.7	5.1	3.3	-0.9	-6.5	-17.4
F-4	0.8	-0.1	0.2	1.5	1.6	-0.5	-9.8
F-5	0.5	2.7	4.3	4.6	1.5	-6.1	-14.6
F-6	0.1	3.1	4.4	3.6	-1.1	-6.8	-15.6
F-7	-8.3	-1.2	2.6	3.7	2.0	-2.6	-11.3
G-1	4.8	5.7	5.5	4.4	1.2	-5.2	-13.8
G-2	7.0	7.6	6.7	4.8	0.7	-7.1	-17.8
G-3	8.2	7.7	6.4	4.0	-0.2	-5.3	-16.0
G-4	4.5	4.1	4.1	3.8	2.5	-1.7	-11.5
G-5	5.6	6.3	6.2	4.7	0.6	-7.0	-14.6
G-6	0.7	1.8	3.8	3.9	0.9	-4.8	-14.2
G-7	-7.5	-2.2	1.6	4.0	2.7	-2.0	-9.4
H-1	11.7	10.0	8.1	6.9	4.7	0.0	-6.7
H-2	12.8	12.3	11.6	9.8	6.5	1.3	-7.9
H-3	13.8	13.1	12.0	9.0	5.6	0.4	-8.4
H-4	11.2	10.8	9.9	8.4	6.1	2.2	-5.1
H-5	12.6	11.9	11.0	8.7	5.8	-1.4	-8.2
H-6	4.8	6.1	6.6	5.9	3.6	0.4	-7.4
H-7	-2.2	0.4	3.6	5.4	4.6	0.8	-4.3
I-1	12.7	9.2	4.8	2.4	-0.4	-2.0	-2.0
I-2	11.2	10.1	7.3	5.2	1.3	-2.6	-4.5
I-3	10.7	9.8	7.5	4.9	2.0	-2.3	-5.3
I-4	8.5	8.0	6.7	4.9	2.4	-1.3	-4.8
I-5	9.0	7.8	6.9	5.8	2.5	-2.7	-5.9
I-6	4.0	3.7	3.4	2.9	0.9	-1.8	-5.1
I-7	-2.5	-1.1	1.1	2.9	2.1	0.2	-2.7

APPENDIX - NOTATION

The following symbols are used in this paper:

B_o = the representative width of a channel;

F_r = the Froude number;

g = the acceleration of gravity;

h = local water depth;

H_o = the representative depth in a bend;

l = length of a straight reach between two neighboring bends;

L = the total path distance along a meander;

n = the lateral coordinate taken perpendicular to s-axis;

p = pressure;

r = local radius of curvature;

r_c = the radius of curvature of the centerline of a meander;

R = the minimum radius of curvature along a meander;

R_e = the Reynolds number;

s = the longitudinal coordinate parallel to the tangent of the centerline of meander;

u_s, u_n = velocity components in s- and n-direction, respectively;

$\bar{u}_s$ = depth-averaged value of u_s;

u_* = shear velocity;

V = the representative mean velocity in a bed;

z = the vertical coordinate taken positively upward;

z_s = the vertical coordinate at the water surface;

δ = angle between velocity vector and s-axis;

ε = eddy vescosity;

ρ = the density of water;

λ = wavelength of a meander;

Θ_b = the angle of the change in the direction through a bend; and

ω = $2\pi/L$.